

# Effect of Pressure Rate on Rate and State Frictional Slip

J. W. Rudnicki<sup>1</sup>, Y. Zhan<sup>2</sup>

<sup>1</sup>Department of Civil and Environmental Engineering and Department of Mechanical Engineering,  
Northwestern University, Evanston, IL 60208-3109

<sup>2</sup>School of Civil and Resource Engineering, University of Science and Technology Beijing, No. 30,  
Xueyuan Road, Haidian District, Beijing, 100083, P. R. China

## Key Points:

- At low pressure rates instabilities are due to rate and state friction
- At high pressure rates failure occurs based on the Coulomb law with the effective stress principle
- Pressure rate affects the type, frequency, and magnitude of slip events

## Abstract

This paper analyzes the effects of pore pressure rate for a spring - block system that is a simple model of a laboratory experiment. Pore pressure is increased at a constant rate in a remote reservoir and slip is governed by rate and state friction. The frequency of rapid slip events increases with the increase of a nondimensional pressure rate that is the ratio of the time scale of frictional sliding to that for pressure increase. Rate and state and pressure rate effects interact in a limited range of pressure rate and diffusivity. Above a critical value of the pressure rate there is transition to a significant downward linear trend of the stress, reflecting the increase of pore fluid pressure in the reservoir. This trend leads to Coulomb failure due to the decrease of the frictional resistance and the effective stress principle.

## Plain Language Summary

Recent field observations have identified fluid injection as an important factor in causing the dramatic increase of earthquakes in the central US and recent laboratory experiments have observed effects of fluid pressure rate on frictional sliding. This paper studies a simple model of a laboratory experiment: a block resting on a frictional surface and pulled by a spring. The frictional resistance to sliding depends on the rate and history of sliding. Fluid pressure is increased at a constant rate at a distance remote from the surface. The paper calculates the types and characteristics of rapid slip events and their dependence on the pressure rate and how fast fluid can diffuse from the reservoir to the frictional surface.

## 1 Introduction

Increases in pore fluid pressure are an important mechanism to promote failure (slip) on fault surfaces. According to the Coulomb condition the frictional resistance is given by

$$\tau = \mu_0 (\sigma - p) \quad (1)$$

where  $\mu_0$  is a friction coefficient,  $\sigma$  is the normal stress on the frictional surface and  $p$  is the pore fluid pressure. The pore fluid pressure reduces the effective normal stress (normal stress minus pore fluid pressure) and thereby reduces the frictional resistance. Slip, which could be seismic or aseismic, is predicted to occur when the applied shear stress equals the resistance.

This mechanism has been suggested as playing an important role in a variety of geologic processes. Much recent attention on the effects of pore fluid on failure has been stimulated by the dramatic increase of earthquakes in the mid-continent US (Ellsworth, 2013). Most of these events appear to be associated with the injection of waste water from hydraulic fracturing (Horton, 2012; Keranen et al., 2013, 2014; Weingarten et al., 2015; Barbour et al., 2017; Goebel et al., 2017) There is not yet any clear understanding of why these earthquakes do or do not occur and whether induced slip will be seismic or aseismic. The nearness of stress on faults to a critical value, the orientation and location of faults relative to injection sites, and availability of permeability channels are certainly factors. Operational factors that affect the incidence of seismicity include the volume of fluids injected or withdrawn and the injection rate (Ellsworth, 2013).

Weingarten et al. (2015) examined about 20,000 wells in the mid-continent US associated with seismicity and found that among various operational parameters, the injection rate had the best correlation with induced seismicity. A computational study by Almakari et al. (2019) examined the effect of pore pressure rate on seismicity. They simulated the seismicity rate increase due to a ramp increase in pore pressure on a heterogeneous fault. They found that a sharp increase in the seismicity rate correlates with

61 the pore pressure rate for a wide range of injection pressure and that the maximum seis-  
62 micity rate increases with the pore pressure rate.

63 Although field observations are the ultimate test of the effects of pore fluid on fail-  
64 ure, their interpretation is often complicated by uncertainty about the boundary con-  
65 ditions, state of stress, heterogeneity of hydrologic and mechanical structure, and his-  
66 tory. Laboratory experiments, despite their limited size and time scales, offer a more con-  
67 trolled environment that can contribute insight into fundamental processes.

68 Recent laboratory studies addressing the role of pressure rate in causing slip are  
69 those of French et al. (2016), Passelégue et al. (2018), Cappa et al. (2019) and Noël et  
70 al. (2019). The primary motivation for this study is the experiments by French et al. (2016).  
71 They did axisymmetric compression tests with saw cuts on two sandstones, Berea and  
72 Darley Dale. In addition to standard axisymmetric compression tests, they did tests in  
73 which the confining stress was reduced or the pore pressure in the reservoir connected  
74 to the sample was increased at a constant rate. In some tests, they did both. They found  
75 that instability (accelerated slip events) did not occur unless they decreased the confin-  
76 ing stress (lateral relaxation tests). When they did get instability, the total slip, slip ve-  
77 locity and shear stress drops of events were better correlated with the pore pressure rate  
78 (in the reservoir) than with the magnitude of the pore pressure itself.

79 This paper extends the spring - block model of Segall and Rice (1995) (Figure 1)  
80 to examine the effect of pressure rate. The spring - block system is an oversimplified model  
81 of crustal faulting, but it is a reasonable idealization of laboratory experiments in which  
82 slip occurs nearly simultaneously on the frictional surface. Segall and Rice (1995) showed  
83 that this system exhibits a wide spectrum of behavior that is further enriched by includ-  
84 ing the pressure rate. Despite the limitations of the model for crustal faulting, among  
85 their results are a constraint on the maximum pore pressure at depth that is consistent  
86 with the absence of an observed heat flow anomaly and the occurrence of aftershock-like  
87 instabilities.

88 The goal of this study is to examine the role of imposed pore pressure rate on fric-  
89 tional slip. The calculations are not meant to be a faithful simulation of the experiment  
90 of French et al. (2016) but their observations are used as a guide. Although French et  
91 al. (2016) discuss some of their results in terms of rate and state (hereafter abbreviated  
92 RS) friction, they do not infer any RS parameters from their experiments. Nevertheless,  
93 we use RS friction because of its strong observational basis and wide use in fault mod-  
94 els. The results can aid in the interpretation of laboratory tests and, to a lesser extent,  
95 field studies.

## 96 2 Formulation

97 The model is that of Segall and Rice (1995) shown in Figure 1. A block of unit area  
98 subjected to a constant normal stress  $\sigma$  slides on a thin porous layer. The block is con-  
99 nected to a spring with stiffness  $k$ . Slip of the block is  $u$ . The other end of the spring  
100 is displaced at a constant rate  $v_0$ . Thus, the shear stress due to motion of the block is

$$101 \quad \tau = k(v_0 t - u) \quad (2)$$

102 The layer has porosity  $\phi$  and a pore pressure  $p$ . There is a flux of fluid to the layer from  
103 a remote reservoir with a pore pressure  $p_\infty$ . The remote reservoir is at some nominal dis-  
104 tance  $L$  from the layer. Consistent with the discrete spring-mass system, Segall and Rice  
105 (1995) adopt the approximation of Rudnicki and Chen (1988) that the fluid mass flux  
106 into the layer is proportional to the difference between the remote pore pressure  $p_\infty$  and  
107 the pore pressure in the layer. Consequently the equation expressing conservation of fluid  
108 mass is

$$109 \quad c^*(p_\infty - p) = \dot{p} + \dot{\phi}/\beta \quad (3)$$

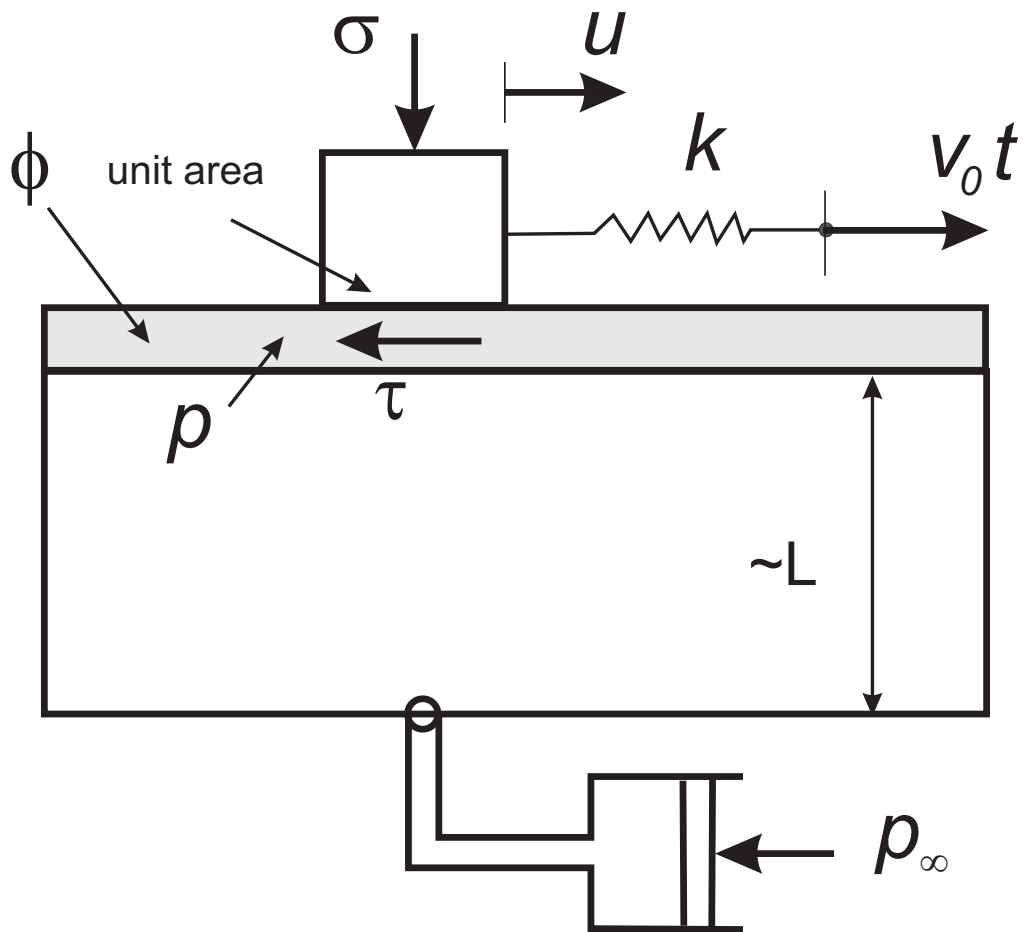


**Figure 1.** The spring - block model of Segall and Rice (1995)

110 where  $\phi$  is now the inelastic part of the porosity, the superposed dot denotes the time  
 111 derivative and  $c^*$  is the reciprocal of a time constant for fluid diffusion.  $c^*$  can be expressed  
 112 in terms of a diffusivity  $c$  as  $c^* = c/L^2$ .  $\beta = \phi_0(\beta_f + \beta_\phi)$  is a compressibility where  
 113  $\beta_f$  is the compressibility of the pore fluid,  $\beta_\phi$  is the compressibility of the pore space and  
 114  $\phi_0$  is the initial porosity. In an extension of Segall and Rice (1995) we take the far-field  
 115 pore pressure to increase linearly with time:

$$116 \quad p_\infty = p_\infty^0 + \dot{p}_\infty t \quad (4)$$

117 Slip on the layer is described by RS friction (Dieterich, 1979; Ruina, 1983) of the  
 118 form

$$119 \quad \tau = (\sigma - p) [\mu_0 + a \ln(v/v_0) + b(\theta/\theta_0)] \quad (5)$$

120 where  $\mu_0$  is the nominal friction coefficient,  $v = du/dt$  is the slider velocity, and  $\theta$  is  
 121 a state variable. Reference values of the velocity and state are  $v_0$  and  $\theta_0$  and  $a$  and  $b$  are  
 122 constitutive parameters. Two versions of the equation for the evolution of state are typ-  
 123 ically used: the “slip” law and the “aging” or “slowness” law. Segall and Rice (1995) use  
 124 the “aging” law:

$$125 \quad \dot{\theta} = 1 - \theta v/d_c \quad (6)$$

126 where  $d_c$  is a characteristic sliding distance.

127 If the block has been steadily sliding at a velocity  $V_1$  and the velocity is suddenly  
 128 changed to a velocity  $V_2 > V_1$ , the friction suddenly increases by  $a \ln(V_2/V_1)$  and then  
 129 decays over a characteristic distance  $d_c$  to a new steady state level  $(b - a) \ln(V_2/V_1)$ . For  
 130  $b - a > 0$  the new steady state level is less than the old and the response is velocity  
 131 weakening. For  $b - a < 0$  the response is velocity strengthening. Ruina (1983) showed  
 132 that for velocity weakening the response can be unstable, in the sense that small per-  
 133 turbations grow exponentially in time, when the spring stiffness is less than a critical value  
 134 given by

$$135 \quad k_{crit} = (\sigma - p)(b - a)/d_c \quad (7)$$

136 Note that the pore pressure can affect stability in two ways. In (7) an increase in  
 137 pore pressure reduces  $k_{crit}$ . However an increase in pore pressure reduces the frictional  
 138 resistance according to (5). Because the magnitudes of  $a$  and  $b$  are small compared with  
 139  $\mu_0$ , the difference between the magnitudes of (5) and (1) is small. Hence, when the pore  
 140 pressure increases sufficiently to reduce the frictional resistance below the applied shear  
 141 stress, failure essentially occurs according to (1). We refer to this as a Coulomb failure.  
 142 The simulations will show that there is a transition from RS instability according to (7)  
 143 to Coulomb failure with increasing pressure rate.

144 Segall and Rice (1995) proposed the following evolution equation for the porosity:

$$145 \quad \dot{\phi} = -(\phi - \phi_{ss})v/d_c \quad (8)$$

146 where the steady state value is given by  $\phi_{ss} = \phi_0 + \varepsilon \ln(v/v_0)$ . The initial value of the  
 147 porosity is  $\phi_0$  and  $\varepsilon$  is a parameter that gives the magnitude of the effect. They show  
 148 that this formulation describes well the data of Marone et al. (1990) on porosity changes  
 149 with shear of simulated fault gouge and find that  $\varepsilon = 1.7 \times 10^{-4}$ .

150 The final ingredient is the equation of motion:

$$151 \quad \dot{\tau} = k(v_0 - v) - \eta \dot{v} \quad (9)$$

152 The second term on the right employs the radiation damping approximation to inertia,  
 153 i.e.  $mdv/dt$  is replaced by  $\eta v$  where  $\eta = G/2v_s$ .  $G$  is the shear modulus and  $v_s$  is the  
 154 shear wave velocity (Rice & Tse, 1986; Rice, 1993).

155 Differentiating (5) and setting equal to (9) along with (3), (6), and (8) yield a sys-  
 156 tem of four ordinary differential equations for  $V$ ,  $p$ ,  $\theta$ , and  $\dot{\phi}$ . It is advantageous to rewrite  
 157 these equations in the non-dimensional variables  $V = v/v_0$ ,  $T = v_0 t/d_c$ ,  $\Sigma = \mu_0(1 - p/\sigma)$ ,  
 158  $P = p/\sigma$ ,  $\hat{\eta} = \eta v_0/\sigma$ ,  $\hat{c} = c^* d_c/v_0$ ,  $\hat{\beta} = \sigma\beta$ ,  $\hat{\theta} = \theta v_0/d_c$ ,  $\hat{\phi} = \phi - \phi_0$  and  $\hat{k} = k/k_c$   
 159 where  $k_c$  is the critical stiffness (7) based on the initial value of the far-field pore pres-  
 160 sure  $p_\infty^0$ . With these non-dimensionalizations  $\dot{P}_\infty = \dot{p}_\infty d_c/v_0\sigma$ .

### 161 3 Parameter Values

162 Although the model is simple, there are a quite a few parameters. Some of these  
 163 are uncertain and others vary widely. In the simulations, we will vary two non-dimensional  
 164 parameters,  $\dot{P}_\infty$  and  $\hat{c}$  to focus on the roles of the pressure rate and diffusivity. To the  
 165 extent possible, we choose values representative of the experiments of French et al. (2016).  
 166 In Table 1, they give imposed slip rates ranging from  $1.6 \times 10^{-7}$  to  $4.6 \times 10^{-7}$  m/s for  
 167 Berea and  $1.6 \times 10^{-7}$  to  $6.5 \times 10^{-7}$  m/s for Darley Dale. We take  $v_0 = 3.0 \times 10^{-7}$   
 168 m/sas representative. Lateral confining stresses range from 42 to 62 MPa and we take  
 169  $\sigma = 50$  MPa. The initial value of the pore pressure is about 10 MPa. This gives  $P_\infty^0 =$   
 170  $0.2$ . Using  $v_s = 2.5 \times 10^3$  m/s (Green & Wang, 1994) and  $G = 10^4$  MPa gives  $\hat{\eta} \approx$   
 171  $10^{-8}$ . Pore pressure rates vary from 0.3 to 1.0 MPa/min.

172 French et al. (2016) give  $10^{-14}$  m<sup>2</sup> and  $10^{-13}$  m<sup>2</sup> for the permeabilities of Berea and  
 173 Darley Dale, respectively. The diffusivity is given by  $c = k\gamma/\nu S$  where  $k$  is the perme-  
 174 ability,  $\gamma$  is the weight density of water ( $9.81 \times 10^4$  Pa),  $\nu$  is the kinematic viscosity of  
 175 water ( $10^{-3}$  Pa s) and  $S$  is a storage coefficient, equal to  $1.5 \times 10^{-6}$  m<sup>-1</sup> (Green & Wang,  
 176 1994). These values give  $c = 0.065$  m<sup>2</sup>/s for Berea. Dividing by the square of the spec-  
 177 imen length (50.8 mm) gives  $c^* = 25.2$  s<sup>-1</sup>.

178 Although French et al. (2016) discuss their results in terms of RS friction, they do  
 179 not measure the parameters in their experiment. Segall and Rice (1995) infer  $d_c = 0.02$ mm  
 180 and  $\epsilon = 1.7 \times 10^{-4}$  from the experiments of Marone et al. (1990) and  $\beta = 1.4 \times 10^{-4}$  MPa<sup>-1</sup>  
 181 from experiments of Zoback and Byerlee (1976) and we use these. Using the larger of  
 182 the pressure rates (1 MPa/min),  $v_0 = 3.0 \times 10^{-7}$  m/s, and  $d_c = 0.02$  mm gives  $P_\infty =$   
 183  $0.022$ .

184 In addition, we adopt the representative RS frictional parameters used by Segall  
 185 and Rice (1995),  $a = 0.010$  and  $b = 0.015$ , and take the nominal coefficient as  $\mu_0 =$   
 186  $0.64$  (French et al., 2016). Because  $a < b$ , the behavior is velocity weakening and a crit-  
 187 ical value of the stiffness is given by (7). In their experiments, French et al. (2016) in-  
 188 duce instability (resulting in rapid slip events) by reducing the lateral confining stress  
 189 leading to a reduction of normal stress on the slip surface. For simplicity and in order  
 190 to focus on the role of the pressure rate, we keep the normal stress  $\sigma$  constant and ex-  
 191 amine the response for values of the stiffness less than the critical value for drained de-  
 192 formation given by (7). In particular, we arbitrarily take  $\hat{k} = 0.1$ . (Results for  $\hat{k} = 0.5$   
 193 are shown in the Supporting Information).

194 Segall and Rice (1995) derive an expression critical stiffness as a function of the non-  
 195 dimensional diffusivity  $\hat{c}$ . When expressed as the ratio to the critical stiffness for drained  
 196 deformation, (7), the result is

$$197 \quad K(\hat{c}) = 1 - \frac{\epsilon\mu_0}{\beta(\sigma - p)(b - a)} F(\hat{c}) \quad (10)$$

198 where  $F(\hat{c}) \rightarrow 0$  as  $\hat{c} \rightarrow \infty$ , corresponding to very rapid diffusion and drained con-  
 199 ditions (pore pressure equal to that in the reservoir), and  $F(\hat{c}) \rightarrow 1$  as  $\hat{c} \rightarrow 0$ , corre-  
 200 sponding to very slow diffusion and undrained conditions (no change in fluid mass).

201 For the values of parameters of the experiment,  $c = 0.065$  m<sup>2</sup>/s,  $v_0 = 3.0 \times 10^{-7}$   
 202 m/s and  $d_c = 0.02$  mm,  $\hat{c} = 1.68 \times 10^3$  and from (10)  $K \approx 1$ , indicating that deforma-

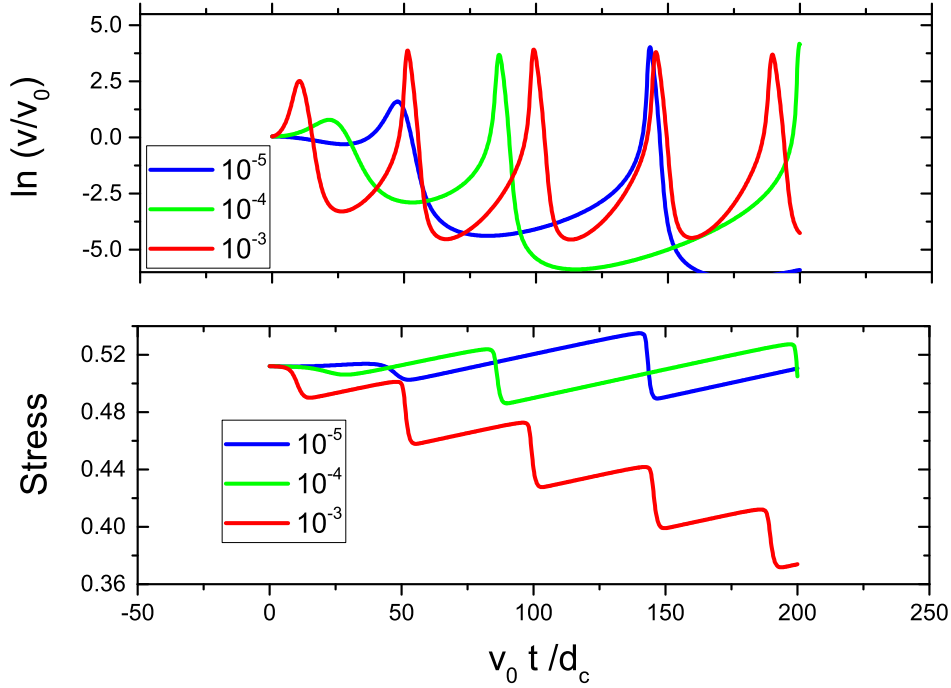


**Figure 2.** Upper panel shows logarithm of velocity (divided by  $v_0$ ) and lower panel shows stress (divided by  $\sigma$ ),  $\Sigma = \mu_0(1 - p/\sigma)$ , for three values of  $\hat{P}_\infty$ :  $10^{-5}$ ,  $10^{-4}$  and  $10^{-3}$ . The abscissa is  $T = v_0 t / d_c$  and  $\hat{c} = 1$ .

203 tion is essentially drained. However, French et al. (2016) cite Zhang and Tullis (1998)  
 204 in arguing that permeabilities could be as small as  $10^{-17} \text{ m}^2$  for gouge layers formed by  
 205 frictional shearing of surfaces and Wibberley and Shimamoto (2003) have found perme-  
 206 abilities as low as  $10^{-19} \text{ m}^2$  in samples from the fault core of the Median Tectonic Line.  
 207 These give values of  $\hat{c}$  three to five orders of magnitude smaller.

#### 208 4 Simulations

209 The simulations are started with a small perturbation from steady sliding:  $v(0) =$   
 210  $1.05v_0$ . Other initial conditions are as follows:  $\tau(0) = \mu_0(\sigma - p_\infty^0)$ ,  $p = p_\infty^0$ ,  $\hat{\phi} = 0$ ,  
 211 and  $\hat{\theta} = v_0/v(0)$ . Results are shown for  $\hat{k} = 0.1$ , three values of  $\hat{P}_\infty$ ,  $10^{-5}$ ,  $10^{-4}$ , and  
 212  $10^{-3}$ , and two values of  $\hat{c}$ : 1.0 (Figure 2) and 10 (Figure 3). The upper panel of Figure  
 213 2 shows a series of rapid slip events. If the first event is ignored (because it appears to  
 214 be affected by the initial conditions), the maximum slip velocity is about 40 ( $e^{3.7}$ ) times  
 215 the imposed velocity. For  $\hat{P}_\infty = 10^{-3}$ , there are three events with periods about 45 but  
 216 only the first, at  $T \approx 52$ , is within the duration of the experiment  $T = 60$  (correspond-  
 217 ing to about 4000 s). For  $\hat{P}_\infty = 10^{-5}$  and  $10^{-4}$  only one event (again ignoring the first)  
 218 occurs within the duration of the simulation. The bottom panel shows the stress. Drops  
 219 occur simultaneously with the slip events. For  $\hat{P}_\infty = 10^{-3}$  the stress drop is about 0.04  
 220 (a dimensional stress drop of  $0.04 \times \sigma = 2 \text{ MPa}$ ). For  $\hat{P}_\infty = 10^{-4}$  the stress drop is  
 221 slightly smaller and slight larger for  $\hat{P}_\infty = 10^{-5}$ . For values of  $\hat{P}_\infty$  less than  $10^{-5}$  the  
 222 effect of the pore pressure rate is minimal and the response is nearly entirely due to RS  
 223 effects. For  $10^{-3}$  the downward trend reflects the linear increase in pore fluid pressure

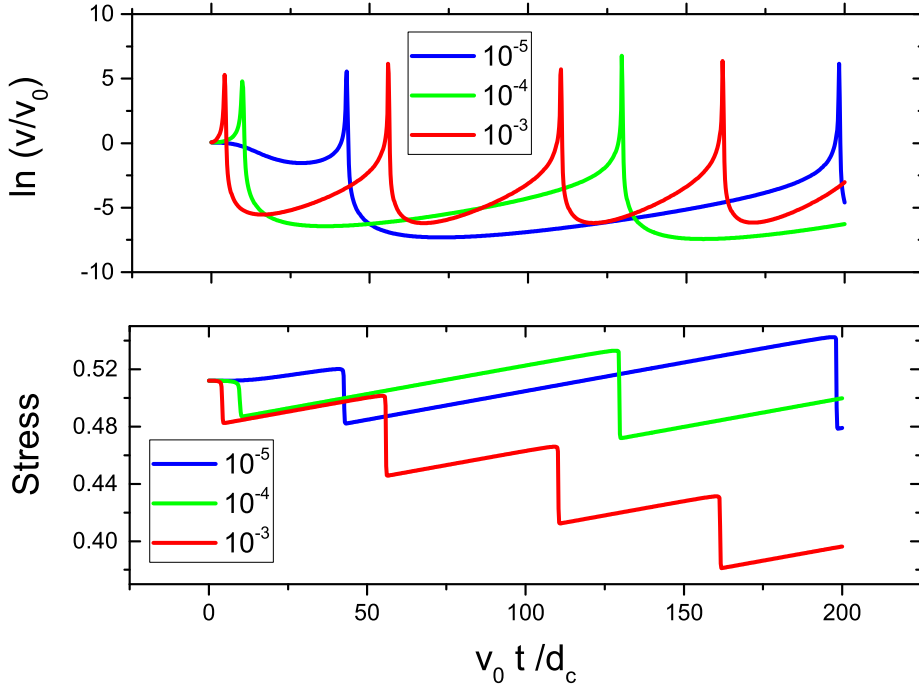


**Figure 3.** Same as Figure 2 for  $\hat{c} = 10$ .

224 in the reservoir. This increase reduces the nominal frictional resistance,  $\mu_0 (\sigma - p)$ , and  
 225 tends toward a Coulomb failure.

226 Figure 3 shows results for  $\hat{c} = 10$ . For  $\dot{P}_\infty = 10^{-3}$  the peak velocities ( $e^5 = 155$ )  
 227 and the stress drops are larger (0.05) and the time between events is longer (52) than  
 228 for  $\hat{c} = 1$ . For  $\dot{P}_\infty = 10^{-4}$  and  $10^{-5}$ , the magnitude of the peak velocity and stress drop  
 229 are slightly larger. If, again, the first slip event is ignored, during the duration of the exper-  
 230 iment only one event occurs for  $\dot{P}_\infty = 10^{-3}$  and none for  $10^{-4}$  and  $10^{-5}$ . As in Fig-  
 231 ure 2, there is a transition at  $\dot{P}_\infty = 10^{-3}$  to a significant downward trend of the stress  
 232 that eventually will reduce the frictional resistance to zero. According to (10), for  $\hat{c} =$   
 233 10, the ratio of the critical stiffness to the critical stiffness for drained deformation (both  
 234 based on the pore pressure  $p_\infty^0$ )  $K = 0.938$ . Therefore,  $\hat{c} = 10$  is close to drained condi-  
 235 tions and there will be little difference in the response for larger values of  $\hat{c}$ . For  $\hat{c} =$   
 236 1,  $K = 0.51$ , which is much closer to undrained response and, according to Figure 4  
 237 of Segall and Rice (1995), is in a range where  $K(\hat{c})$  decreases rapidly with  $\ln(\hat{c})$ . For the  
 238 parameters here undrained deformation is stable and the response is increasingly damped  
 239 for smaller values of  $\hat{c}$ . Thus, the smaller peak velocities and stress drops in Figure 2,  
 240  $\hat{c} = 1$ , compared with Figure 3,  $\hat{c} = 10$ , reflect the stabilizing effects of dilatant hard-  
 241 ening for conditions closer to undrained deformation. (Results for  $\hat{c} = 0.1$  are shown  
 242 in Supporting Information.)

243 For  $\dot{P}_\infty = 10^{-2}$ , representative of the laboratory value, the frictional resistance  
 244 decreases to zero before the end of the simulation ( $T = 200$ ) but does not for  $T = 60$ ,  
 245 corresponding to the duration of the experiment. Figure 4 shows the response for two  
 246 values of  $\hat{c}$ : 1 and 10. For the larger diffusivity there are 11 slip events with slightly de-  
 247 creasing maximum slip rates. For  $\hat{c} = 1$ , there is a single slow event followed by strongly  
 248 damped oscillations. For smaller diffusivities, the response is even more strongly damped.

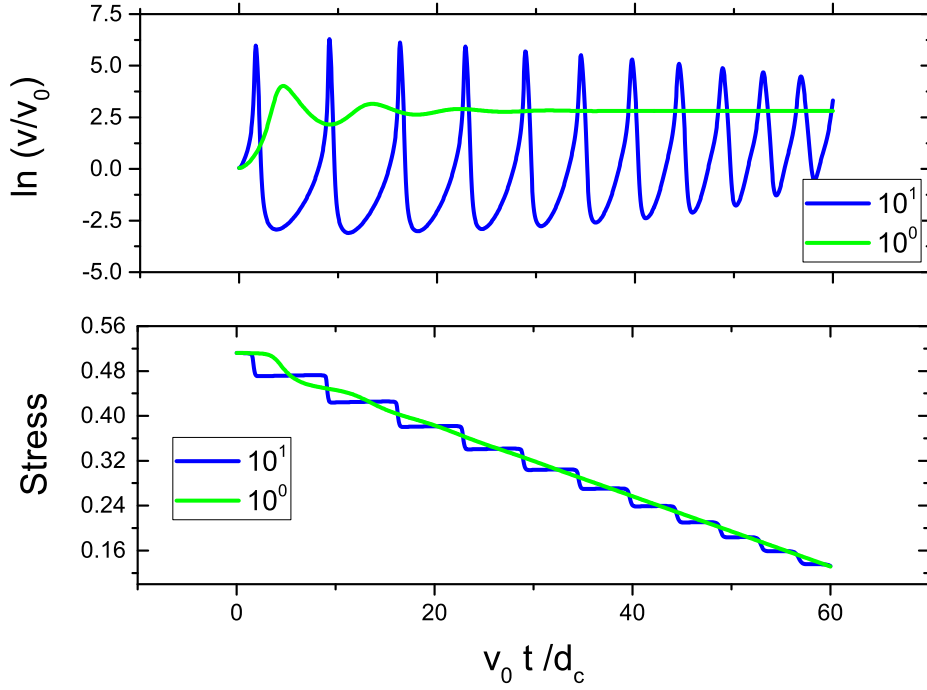


**Figure 4.** Same as Figure 2 for  $\dot{P}_\infty = 10^{-2}$  and  $\hat{c} = 1$  and 10.

249 The lower panel shows that the relatively rapid increase of pressure causes a steep, linear  
 250 downward trend of the stress that will reach zero shortly after  $T = 60$ .

## 251 5 Discussion

252 The simulations illustrate the effects of  $\dot{P}_\infty$ , the ratio of the characteristic time of  
 253 the imposed rate of frictional slip to that of pressurization. For all the values of  $\hat{c}$  and  
 254  $\hat{k}$  considered, the frequency of events increases with  $\dot{P}_\infty$ . Also, in all cases, between  $\dot{P}_\infty =$   
 255  $10^{-4}$  and  $10^{-3}$  there is transition to a significant downward linear trend of the stress,  
 256 reflecting the linear increase of pore fluid pressure in the reservoir. This trend leads to  
 257 Coulomb failure due to the decrease of the frictional resistance according to the effective  
 258 stress principle. For  $\dot{P}_\infty$  within the range of  $10^{-5}$  to  $10^{-3}$  the interaction of RS ef-  
 259 fects and the increase of pore pressure is most significant. For values smaller than about  
 260  $10^{-5}$  the pressure rate has relatively little effect and the occurrence of slip events is do-  
 261 minated by RS effects.

262 The response also depends on  $\hat{c}$ , the ratio of the characteristic time of the imposed  
 263 rate of frictional slip to that of fluid diffusion. The magnitude of the stress drop and peak  
 264 velocities decrease with decreasing  $\hat{c}$ . The decrease is most dramatic for  $\hat{c} = 0.1$ , reflect-  
 265 ing the stabilizing effect of dilatant hardening as undrained conditions are approached.  
 266 This stabilizing effect begins to dominate for  $\hat{c}$  less than about 1. For  $\hat{c}$  greater than about  
 267 10 conditions are effectively drained and largely independent of  $\hat{c}$ . Despite the simplic-  
 268 ity of the model, these results inform the range of parameters for which different effects  
 269 dominate and indicate a transition from RS instability to Coulomb failure with increas-  
 270 ing  $\dot{P}_\infty$ .

271 Although the spring-slider system is a reasonable approximation of a laboratory  
 272 test, the calculations here cannot be considered a faithful simulation of the experiments  
 273 of French et al. (2016). A major difference is that for simplicity and to isolate the effect  
 274 of the reservoir pressure rate we have taken the normal stress as constant. In their ex-  
 275 periments French et al. (2016) alter the normal stress and, in addition, the normal stress  
 276 changes with slip on the frictional surface. Rudnicki and Chen (1988) have used a slip-  
 277 weakening model to examine the interaction of pore pressure effects with normal stress  
 278 changes in experiments by Brace and Martin (1968) and Chambon and Rudnicki (2001)  
 279 extended Segall and Rice (1995) to include normal stress changes. Neither of these stud-  
 280 ies included the pore pressure rate changes or the rate and state effect of changes in the  
 281 normal stress identified by Linker and Dieterich (1992). Although it has been suggested  
 282 that the latter effects are small (Segall & Rice, 1995; Chambon & Rudnicki, 2001), He  
 283 and Wong (2014) have shown that they can significantly affect the slip velocities for state  
 284 evolution described by the slip law.

285 French et al. (2016) give some interpretation of their results in terms of RS effects  
 286 but they do not measure values of the parameters  $a$ ,  $b$  and  $d_c$  and the appropriate val-  
 287 ues are uncertain. Marone et al. (1990) conducted velocity stepping experiments on gouge  
 288 layers of Ottawa sand and the value of  $d_c = 0.02$  mm, inferred by Segall and Rice (1995)  
 289 from their experiments, is probably reasonable for a sandstone. For  $a$  and  $b$  we have sim-  
 290 ply used representative magnitudes with  $b > a$  in order to have velocity weakening and  
 291 instability. It is quite possible and, perhaps, even likely that  $b < a$  and instability is  
 292 induced by changes in normal stress. Furthermore, there are indications that the values  
 293 of  $a$ ,  $b$  and  $d_c$  change with pore pressure and imposed slip rate (Scuderi & Collettini, 2016;  
 294 Noël et al., 2019; Cappa et al., 2019).

295 In spite of the differences between the model and the experiment of French et al.  
 296 (2016) the calculated stress drops, maximum slip rates and number of events are con-  
 297 sistent with those observed in the experiments. For  $\hat{c} = 10$  and  $\dot{P}_\infty = 10^{-3}$  maximum  
 298 slip rates are about two orders of magnitude greater than  $v_0$ , in rough agreement with  
 299 the experiment (Figure 3d of French et al. (2016)). Similarly, stress drops from the cal-  
 300 culations are similar to those in the experiments. Stress drops from Figure 4c of French  
 301 et al. (2016) are 0.5 to 2.0 MPa. In the calculations they are slightly larger, about 2.0  
 302 to 4.0 MPa ( $0.04$  to  $0.05 \times 50$  MPa). In addition, the single slip event predicted during  
 303 the experiment is consistent with the observations. Admittedly, this agreement is based  
 304 on the arbitrary choice of  $\hat{k} = 0.1$ . The response for  $\hat{k} = 0.5$  is not anything like the  
 305 experiment (See Supporting Information.)

306 There are, however, some clear discrepancies between the experiment and the sim-  
 307 ulations. French et al. (2016) observe a pore pressure increase, indicating compaction,  
 308 accompanies slip instability. The magnitude of the decrease is about 55 % of the shear  
 309 stress drop and the increase is permanent. The simulations show a decrease of pressure  
 310 with instability and then an increase with magnitude much smaller than observed in the  
 311 experiment. One possible explanation is that the (nondimensional) pressure rate in the  
 312 experiment is about  $10^{-2}$  at which we find that Coulomb failure begins to dominate RS  
 313 effects. Compaction and dilation in the formulation here, and in Segall and Rice (1995),  
 314 are entirely associated with RS effects. The compaction observed by French et al. (2016)  
 315 could be associated with slip due to the decreasing Coulomb resistance. Alternatively,  
 316 it may be due to the neglect of normal stress changes in the simulations.

317 Another experiment imposing a pore pressure rate is that of Noël et al. (2019). They  
 318 impose a sinusoidal pressure variation with period  $t_0 = 102$  s and amplitudes 1 to 8 MPa  
 319 on a faulted Fontainebleu sandstone. The confining pressure is 30 or 45 MPa, the ax-  
 320 ial displacement rate is  $10^{-3}$  or  $10^{-4}$  mm/s and  $d_c$  decreases from  $4 \times 10^{-3}$  to  $10^{-3}$  mm  
 321 over a velocity range  $10^{-5}$  to  $10^{-2}$  mm/s. Calculating the maximum pressure rate for  
 322 an amplitude of 1 MPa, a confining stress of 40 MPa,  $v_0 = 10^{-4}$  mm/s and  $d_c = 10^{-3}$   
 323 mm gives  $\dot{P}_\infty$  in the range 0.015 to 0.120. At the higher displacement rate  $\dot{P}_\infty$  is an or-

324 der of magnitude higher. They find  $c^* > 1 \text{ s}^{-1}$  and using the same values of  $d_c$  and  $v_0$   
 325 gives  $\hat{c} > 10$ , corresponding to effectively drained conditions. The range of  $\dot{P}_\infty$  is where  
 326 the Coulomb failure dominates instability due to rate and state effects. These estimates  
 327 are consistent with their conclusion that slip instabilities correspond to Coulomb fail-  
 328 ure and that larger amplitudes induce the instability earlier.

329 The spring mass system is a primitive model of faulting. Realistic models of in situ  
 330 slip would include the propagation of slip, inhomogeneity of stress and flux of pore fluid  
 331 along the failure surface (e.g, Garagash and Germanovich (2012), Bhattacharya and Vi-  
 332 esca (2019), Cappa et al. (2019)). Nevertheless, we can make some connection with the  
 333 study of Almakari et al. (2019). They simulate slip on a heterogeneous fault governed  
 334 by rate and state friction and examine the seismicity rate increase due to a ramp increase  
 335 in pore pressure at an injection site. The rates range from 0.01 to 10 MPa/d. They find  
 336 that the seismicity rate increases with both pore pressure and rate, but that the effect  
 337 of the rate is greater. Almakari et al. (2019) use  $\sigma = 100 \text{ MPa}$  and  $v_0 = 10^{-9} \text{ m/s}$ .  
 338 Their values of  $d_c$  vary along the fault and range from 0.01 to 0.37 mm. Using a value  
 339 of  $d_c = 0.1 \text{ mm}$ , in the middle of this range, a pressure rate 10 MPa/d and the values  
 340 of  $\sigma$  and  $v_\infty$  yield  $\dot{P}_\infty = 0.012$ . This is about the same as for the French et al. (2016)  
 341 experiment and at the upper range of where there is a competition between slip events  
 342 due to rate and state friction and a Coulomb failure.

## 343 6 Conclusion

344 We have investigated the system of a spring and a mass sliding on a surface gov-  
 345 erned by rate and state friction. The pore pressure on the surface is coupled to the value  
 346 in a remote reservoir. As Segall and Rice (1995) have shown, the model, although very  
 347 simple, has a rich range of responses. The effects of increasing pore pressure in the reser-  
 348 voir further enrich this range. The analysis is motivated by observations that induced  
 349 seismicity depends on injection rate and, more specifically, by experiments of French et  
 350 al. (2016). The simulations illustrate the effects of pressure rate and diffusivity on the  
 351 type, magnitude, frequency, and stress drop of instabilities. In addition, they identify a  
 352 particular pressure rate at which RS instabilities transition to Coulomb failure. This pres-  
 353 sure rate is similar to those imposed in some experiments and at least one field simu-  
 354 lation. Although the spring block configuration is simple, these simulations can aid in  
 355 the interpretation of experiments and provide guidance for field studies.

## 356 Acknowledgments

357 No new data was used in this manuscript. Y.Z. thanks the University of Science and Tech-  
 358 nology Beijing for support and Northwestern University for hosting him during his visit  
 359 from July 1, 2018 to January 1, 2019.

## 360 References

- 361 Almakari, M., Dublanchet, P., Hervé, C., & Frédéric, P. (2019). Effect of the  
 362 injection scenario on the rate and magnitude content of injection-induced seis-  
 363 micity: case of a heterogeneous fault. *Journal of Geophysical Research*, *124*,  
 364 8426-8448. doi: <https://doi.org/10.1029/2019jb017898>
- 365 Barbour, A. J., Norbeck, J. H., & Rubinstein, J. L. (2017). The effects of vary-  
 366 ing injection rates in Osage County, Oklahoma, on the 2016 Mw 5.8 Pawnee  
 367 earthquake. *Seismological Research Letters*, *140-153*(4), 38.
- 368 Bhattacharya, P., & Viesca, R. C. (2019). Fluid-induced aseismic fault slip outpaces  
 369 pore-fluid migration. *Science*, *364*, 464-468. doi: 10.1126/science.aaw7354
- 370 Brace, W. F., & Martin, R. J., III. (1968). A test of the law of effective stress for  
 371 crystalline rocks of low porosity. *International Journal of Rock Mechanics and*

- 372 *Mining Sciences*, 5, 415-426.
- 373 Cappa, F., Scuderi, M. M., Collettini, C., Guglielmi, Y., & Avouac, J.-P. (2019).  
374 Stabilization of fault slip by fluid injection in the laboratory and in situ. *Sci-*  
375 *ence Advances*, 5(eaau4065). doi: 10.1126/sciadv.aau4065
- 376 Chambon, G., & Rudnicki, J. W. (2001). Effects of normal stress variations on  
377 frictional stability of a fluid-infiltrated fault. *Journal of Geophysical Research*,  
378 106(B6), 11,353-11,372.
- 379 Dieterich, J. H. (1979). Modeling of rock friction, 1, experimental results and consti-  
380 tutive equations. *Journal of Geophysical Research*, 84, 2161-2168.
- 381 Ellsworth, W. L. (2013). Injection-induced earthquakes. *Science*, 341. doi: 10.1126/  
382 science.1225942
- 383 French, M. E., Zhu, W., & Banker, J. (2016). Fault slip controlled by stress path  
384 and fluid pressurization rate. *Geophysical Research Letters*, 43, 4330-4339. doi:  
385 doi:10.1002/2016GL068893
- 386 Garagash, D. I., & Germanovich, L. N. (2012). Nucleation and arrest of dynamic  
387 slip on a pressurized fault. *Journal of Geophysical Research*, 117(B10319). doi:  
388 10.1029/2012JB009209
- 389 Goebel, T. H. W., Weingarten, M., X., C., Haffener, J., & Brodsky, E. E. (2017).  
390 The 2016 Mw 5.1 Fairview, Oklahoma earthquakes: Evidence for long-  
391 range poroelastic triggering at > 40 km from fluid disposal wells. *Earth*  
392 *and Planetary Science Letters*, 472, 50-61. doi: http://dx.doi.org/10.1016/  
393 j.epsl.2017.05.011
- 394 Green, D. H., & Wang, H. F. (1994). Shear wave velocity and attenuation from  
395 pulse-echo studies of Berea sandstone. *Journal of Geophysical Research*,  
396 99(B6), 11755 - 11763. doi: 10:10.1029/94JB00506
- 397 He, C., & Wong, T.-F. (2014). Effect of varying normal stress on stability and  
398 dynamic motion of a spring - slider system with rate- and state- dependent  
399 friction. *Earthquake Science*, 27, 577-587. doi: 10.1007/s11589-014-0098-4
- 400 Horton, S. (2012). Disposal of hydrofracking waste fluid by injection into subsur-  
401 face aquifers triggers earthquake swarm in central Arkansas with potential for  
402 damaging earthquake. *Seismological Research Letters*, 83(2), 250-260. doi:  
403 doi:10.1785/gssrl.83.2.250
- 404 Keranen, K. M., Savage, H. M., Abers, G. A., & Cochran, E. S. (2013). Potentially  
405 induced earthquakes in Oklahoma, USA: Links between wastewater injection  
406 and the 2011 Mw 5.7 earthquake sequence. *Geology*, 41(6), 699-702. doi:  
407 doi:10.1130G34045.1
- 408 Keranen, K. M., Weingarten, M., Abers, G. A., Bekins, B. A., & Ge, S. (2014).  
409 Sharp increase in central Oklahoma seismicity since 2008 induced by mas-  
410 sive wastewater injection. *Science*, 345(6195), 448-451. doi: doi:10.1126/  
411 science.1255802
- 412 Linker, M. F., & Dieterich, J. H. (1992). Effects of variable normal stress on rock  
413 friction: observations and constitutive equations. *Journal of Geophysical Re-*  
414 *search*, 97, 4923-4940.
- 415 Marone, C., Raleigh, C. B., & Scholz, C. H. (1990). Frictional behavior and consti-  
416 tutive modeling modeling of simulated fault gouge. *Journal of Geophysical Re-*  
417 *search*, 95, 7007 - 7025.
- 418 Noël, C., Passelégue, F. X., Giorgetti, C., & Violay, M. (2019). Fault reactivation  
419 during fluid pressure oscillations: Transition from stable to unstable slip. *Jour-*  
420 *nal of Geophysical Research*, 124, 10,940-10,953. doi: https://doi.org/10.1029/  
421 2019JB018517
- 422 Passelégue, F. X., Brantut, N., & Mitchell, T. M. (2018). Fault reactivation by fluid  
423 injection: controls from stress state and injection rate. *Geophysical Research*  
424 *Letters*, 45, 12,837-12846. doi: https://doi.org/10.1029/2018GL080470
- 425 Rice, J. R. (1993). Spatio-temporal complexity of slip on a fault. *Journal of Geo-*  
426 *physical Research*, 98(B6), 9885-9907.

- 427 Rice, J. R., & Tse, S. T. (1986). Dynamic motion of a single degree of freedom sys-  
428 tem following a rate and state dependent friction law. *Journal of Geophysical*  
429 *Research*, *91*(B1), 521-530.
- 430 Rudnicki, J. W., & Chen, C.-H. (1988). Stabilization of rapid frictional slip on a  
431 weakening fault by dilatant hardening. *Journal of Geophysical Research*, *93*,  
432 4745-4757.
- 433 Ruina, A. (1983). Slip instability and state variable friction laws. *Journal of Geo-*  
434 *physical Research*, *88*, 10,359-10,370.
- 435 Scuderi, M. M., & Collettini, C. (2016). The role of fluid pressure in induced vs.  
436 triggered seismicity: insights from rock deformation experiments on carbon-  
437 ates. *Nature Scientific Reports*. doi: 10.1038/srep24852
- 438 Segall, P., & Rice, J. R. (1995). Dilatancy, compaction, and slip instability of a  
439 fluid-infiltrated fault. *Journal of Geophysical Research*, *100*(B11), 22155-  
440 22171.
- 441 Weingarten, M., Ge, S., Godt, J. W., Bekins, B. A., & Rubinstein, J. L. (2015).  
442 High-rate injection is associated with the increase in U.S. mid-continent seis-  
443 micity. *Science*, *348*(6241), 1336-1340.
- 444 Wibberley, C. A. J., & Shimamoto, T. (2003). Internal structure and permeability  
445 of major fault zones: The Median Tectonic Line in Mie Prefecture, Southwest  
446 Japan. *Journal of Structural Geology*, *25*, 49-78.
- 447 Zhang, S., & Tullis, T. (1998). The effect of fault slip on permeability and perme-  
448 ability anisotropy in quartz gouge. *Tectonophysics*, *298*(1-2), 41-52.
- 449 Zoback, M. D., & Byerlee, J. D. (1976). Effect of high-pressure on permeability  
450 of Ottawa sand. *American Association of Petroleum Geologists Bulletin*, *60*,  
451 1531-1542.